DOI: 10.1002/chem.200500937

Systematic Investigation of the Formation of 1D α-Si_3N_4 Nanostructures by Using a Thermal-Decomposition/Nitridation Process

Guozhen Shen,* Yoshio Bando, Baodan Liu, Chengchun Tang, Qing Huang, and Dmitri Golberg[a]

Abstract: This article describes a simple thermal-decomposition/nitridation method for the large-scale synthesis of 1D α-Si_3N_4 nanostructures, such as millimeter-scale microribbons, nanosaws, nanoribbons, and nanowires. These nanostructures are systematically investigated by checking the product deposited at different areas by using powder X-ray diffraction, scanning electron microscopy, transmission electron microscopy, and electron energy loss spectroscopy. Studies show that all these nanostructures have a single-crystalline nature and predominately grow along the [011] direction. These 1D nanostructures are formed by thermal decomposition, followed by the nitridation of SiO.

Keywords: crystal growth · electron microscopy · nanostructures · nitrides · silicon

Introduction

1D nanostructures (wires, rods, tubes, belts, and ribbons) are expected to play an important role in the fabrication of nanoscale devices.[1–3] The utilization of nanoscale materials inevitably requires full control of the structure, size, shape, and the assembly mechanisms, because the intrinsic properties of nanoscale materials are determined by their structures, that is, size, shape, composition, and crystallinity.[4–6] Si_3N_4 is an advanced material and usually two types of structural modifications exist, namely, metastable, low-temperature-phase trigonal α-Si_3N_4 (space group:$P\bar{3}1c$), and stable hexagonal β-Si_3N_4 (space group: $P6_3/m$).[7] Si_3N_4 is one of the most important technical ceramics owing to its interesting properties, such as high strength at high temperatures, low density, good resistance to corrosion, wear, thermal shock and creep, excellent chemical stability, and so forth. These properties favor Si_3N_4 as a suitable material for a wide range of technical applications, especially for high-temperature engineering applications.[8,9]

Much research has focused on the synthesis of 1D Si_3N_4 nanostructures. For example, Si_3N_4 nanowires have been synthesized by using various methods, including a carbon-nanotube-confined reaction, heat treatment of Si and/or SiO_2 with N_2, or combustion with or without catalysts, and so forth.[10,11] Recently, distinct micro- and nanostructures with belt- or ribbonlike morphology in inorganic materials have received extensive attention for both fundamental research and technological applications.[1b,12–14] It is thought that if single-crystalline Si_3N_4 micro- or nanoribbons can be achieved, they will not only possess more interesting mechanical properties, but will also have different optical properties. Si_3N_4 micro- and nanoribbons have been fabricated very recently. For example, An and co-workers synthesized a mixture of α- and β-Si_3N_4 nanobelts through catalyst-assisted pyrolysis of polysilazane.[15] Yin et al. fabricated wide α-Si_3N_4 nanobelts by a vapor–solid (VS) thermal reaction between ammonia and SiO without using a catalyst.[16] Recently, we have reported a very simple and effective thermal-decomposition/nitridation method for the synthesis of Si_3N_4 microribbons, both pure α-Si_3N_4 microribbons and a mixture of α- and β-Si_3N_4 microribbons.[17] In our previous study, we only obtained microribbons of Si_3N_4 and simply investigated their cathodoluminescence properties. In the present work, after systematic investigation of a series of products obtained by designing different deposition crucibles or controlling the experimental parameters, we found that various 1D pure α-Si_3N_4 nanostructures, including millimeter-scale microribbons, nanosaws, nanoribbons, and nanowires, could be obtained by using a simple thermal-decomposition/nitridation method. We studied the photoluminescence (PL) properties of the resulting nanostructures. These

[a] Dr. G. Shen, Prof. Y. Bando, B. Liu, Dr. C. Tang, Dr. Q. Huang, Prof. D. Golberg
Advanced Materials Laboratory
National Institute for Materials Science (NIMS)
Namiki 1-1, Tsukuba, Ibaraki 305-0044 (Japan)
Fax: (+81)29-851-6280
E-mail: shen.guozhen@nims.go.jp

systematic studies of 1D pure α-Si_3N_4 nanostructures may not only provide more comprehensive insights into the formation mechanism of the nanostructures, but may also provide a simple approach to achieve 1D nanostructures with different morphologies.

Results and Discussion

1D Si_3N_4 nanostructures were synthesized in a vertical induction furnace as shown in Figure 1. Following the reaction, it was found that large amounts of white to grey-white

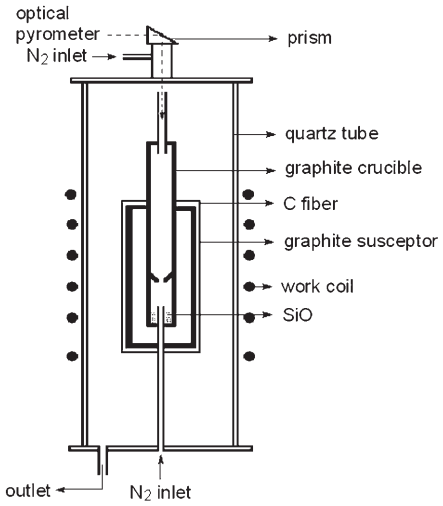

Figure 1. Schematic diagram of the vertical induction furnace utilized in the experiments.

cottonlike fibers grew on the inner wall of the graphite crucible. Figure 2 displays a typical X-ray diffraction (XRD) pattern of the products. All peaks in this pattern can be readily indexed to hexagonal α-Si_3N_4 structures with cell constants comparable to those previously reported in literature (JCPDS No. 41-360). No characteristic peaks from impurities, such as Si, SiO, or SiC were detected in the XRD pattern, indicating the formation of pure α-Si_3N_4 within experimental error (~5%).

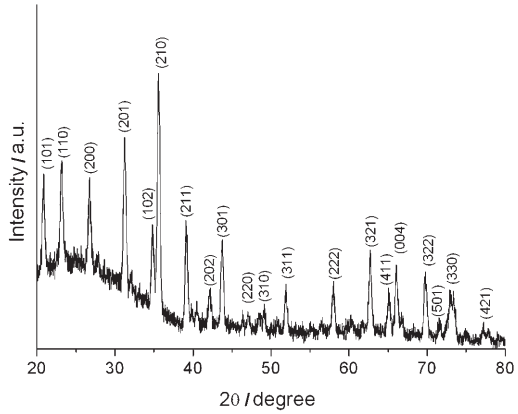

Figure 2. A typical XRD pattern of the product obtained during high-temperature evaporation of SiO in N_2 gas.

The structures and morphologies of the deposited products were further investigated by using scanning electron microscopy (SEM), transmission electron microscopy (TEM), and electron energy loss spectroscopy (EELS). The results show that several unique 1D α-Si_3N_4 nanostructures, including millimeter-scale microribbons, nanosaws, wide nanoribbons, narrow nanoribbons, and nanowires, were deposited on different areas of the inner walls of the crucible; the relationship between the deposition sites and the products are listed in Table 1.

Table 1. The relationship between the deposition distance (between the source material and the deposition site) and the morphology of the product.

Sample Name	Distance [cm]	Product
S1	0	millimeter-scale Si_3N_4 microribbons
S2	~7	Si_3N_4 nanosaws
S3	8–9	wide Si_3N_4 nanoribbons
S4	9–11	narrow Si_3N_4 nanoribbons
S5	~13	Si_3N_4 nanowires

Millimeter-scale α-Si_3N_4 microribbons (S1): Figure 3A shows a low-magnification SEM image of the product directly deposited on the surface of the source materials. The product

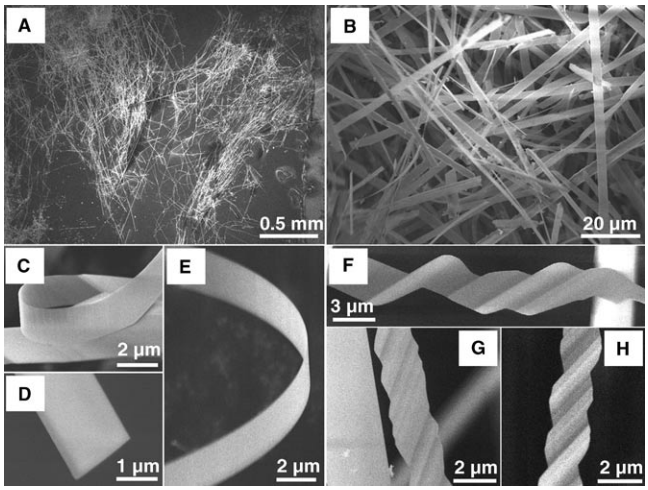

Figure 3. A) Low-magnification and B) high-magnification SEM image of the millimeter-long α-Si_3N_4 microribbons. C–E) SEM images showing the twisted ribbonlike shapes. F–H) Interesting wavy or zigzag microribbons.

consists of a large quantity of very long and straight fiberlike structures. The typical length of the product is several millimeters. The higher magnification SEM image shown in Figure 3B indicates that these fiberlike structures are microribbons with rectangular cross sections. Analysis of a number of the microribbons shows that each microribbon

has a diameter of about 2–7 μm and a thickness of about 200 nm. Figures 3C and D are high-magnification SEM images, which clearly show the twisted ribbon shape and the thickness of the microribbons. During the SEM observations, in addition to the significant portion of Si_3N_4 microribbons shown in Figures 3A–D, the most striking feature is the formation of wavy or zigzag microribbons. Figures 3E and F show the SEM images of wavy or zigzag microribbons. Each microribbon with rectangular cross section is several micrometers in width, 200 nm in thickness and several millimeters in length, Figures 3A–D.

α-Si_3N_4 nanosaws (S2): Recently, very interesting asymmetrically grown 1D nanostructures called nanosaws have been reported for Group 2–6 semiconductors, such as ZnO, CdS, and CdSe.[18] The characteristic feature of these nanosaws is the formation of sawlike ribbons; one side is flat and the other side has sharp or flat teeth. Studies have shown that the nanosaw structures are the result of surface-termination-induced growth; these nanosaw structures are characteristic of semiconductors with wurtzite structure. This observation was also confirmed by the successful fabrication of wurtzite GaN nanosaws.[19] In our experiments, sawlike α-Si_3N_4 nanostructures were also obtained for the first time. The SEM images of the α-Si_3N_4 nanosaws deposited about 7 cm away from the source material are shown in Figures 4A and B. From these images, it is clear that the most dominant morphology found in the as-grown sample is the saw-shaped nanoribbons. Compared with the previously reported nanoribbons or microribbons, the present α-Si_3N_4 nanosaws have one flat side and one sharp, teethlike side instead of two flat sides. The thickness of a typical nanosaw is about 90 nm, as shown in the inset of Figure 4B.

These interesting α-Si_3N_4 nanosaw structures were further investigated by using TEM; the corresponding images are shown in Figures 5A–D. From these images, it can be seen that the width of the nanosaws is about 3–5 μm. The nanosaws are almost transparent as the copper grid can even be seen through several thin nanosaws. The tips of the nanosaws are flat and no particles were found attached to the tips, indicating that the vapor–liquid–solid (VLS) process may not be the dominant growth mechanism for the growth of α-Si_3N_4 nanosaws. The apparent ripplelike contrast in the TEM images is due to the strain resulting from the ribbon bending. The ribbon-shaped structures can also be clearly seen in the the inset of Figure 5C. The inset of Figure 5D is the corresponding selected-area electron diffraction (SAED) pattern of the nanosaw shown in Figure 5D. The

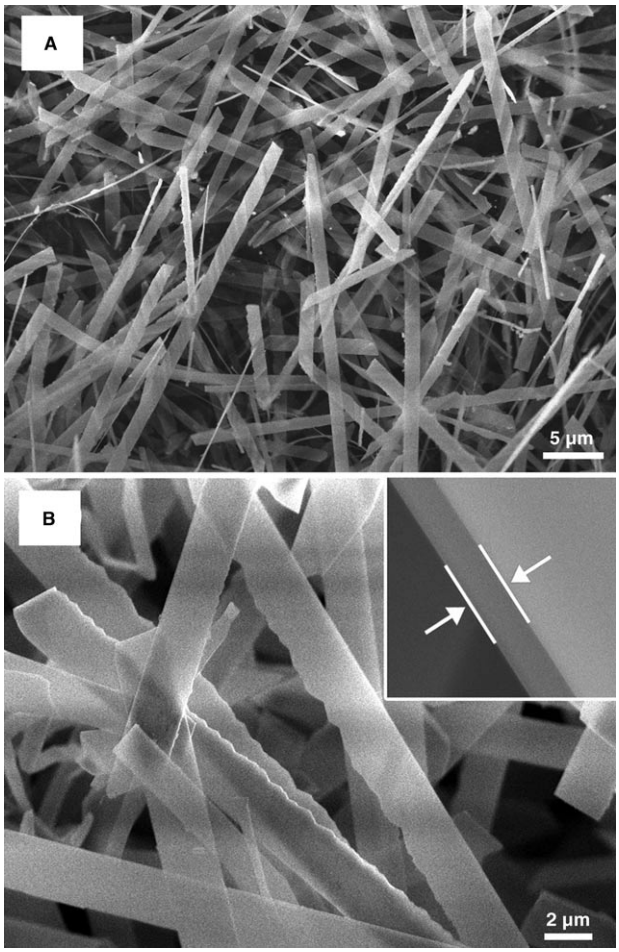

Figure 4. A) Low- and B) high-magnification SEM images of as-grown α-Si_3N_4 nanosaws. The upper right inset in B) shows the typical thickness of a nanosaw.

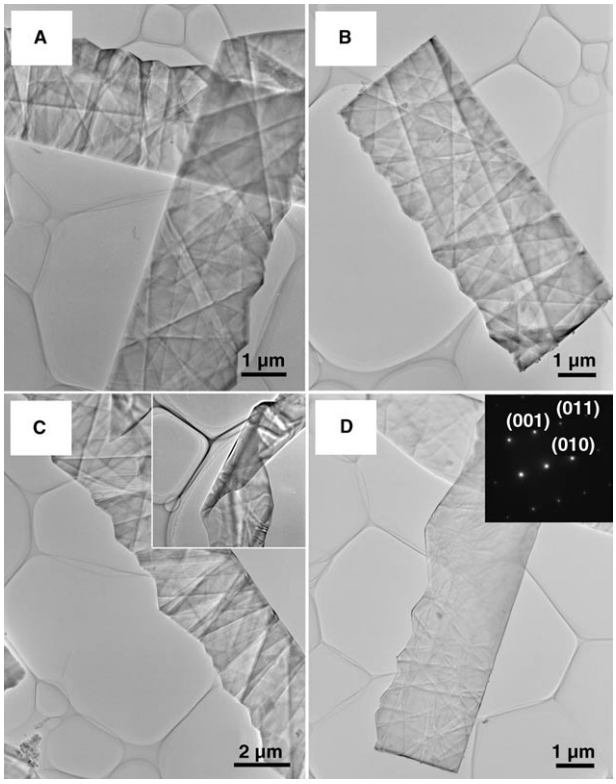

Figure 5. A–D) TEM images of the as-grown α-Si_3N_4 nanosaws. The upper right insets in C) and D) show the ribbon shape and the SAED pattern, respectively.

SAED pattern was obtained from the [100] zone axis of the α-Si_3N_4 nanosaws, which corresponds to the nanobelt grown along the [011] direction. Upon careful checking of several tens of nanosaws it was found that all the α-Si_3N_4 nanosaws have a unique growth along the [011] direction.

Figure 6A is a TEM image of a typical segment of α-Si_3N_4 nanosaws with a diameter of about 3 μm. A representative

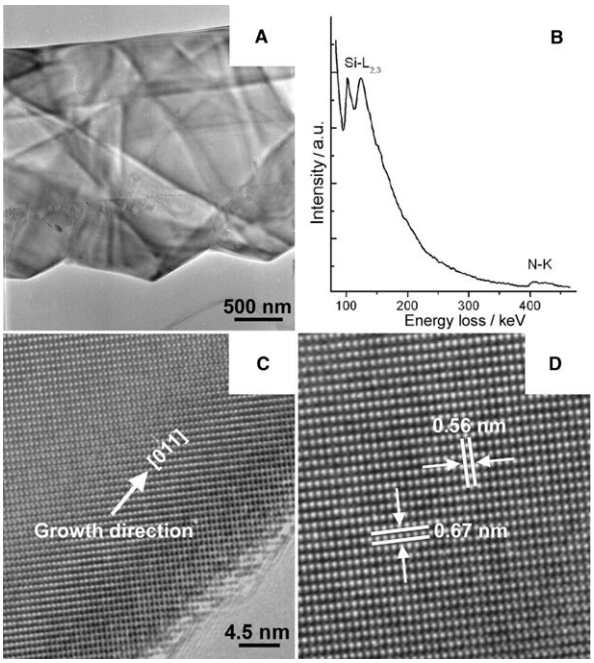

Figure 6. A) A typical low-magnification TEM image of wide α-Si_3N_4 nanosaws. B) EELS spectrum showing that the nanosaws are composed of only two Si and N elements. C) and D) HRTEM lattice images of the α-Si_3N_4 nanosaws grown along the [011] direction.

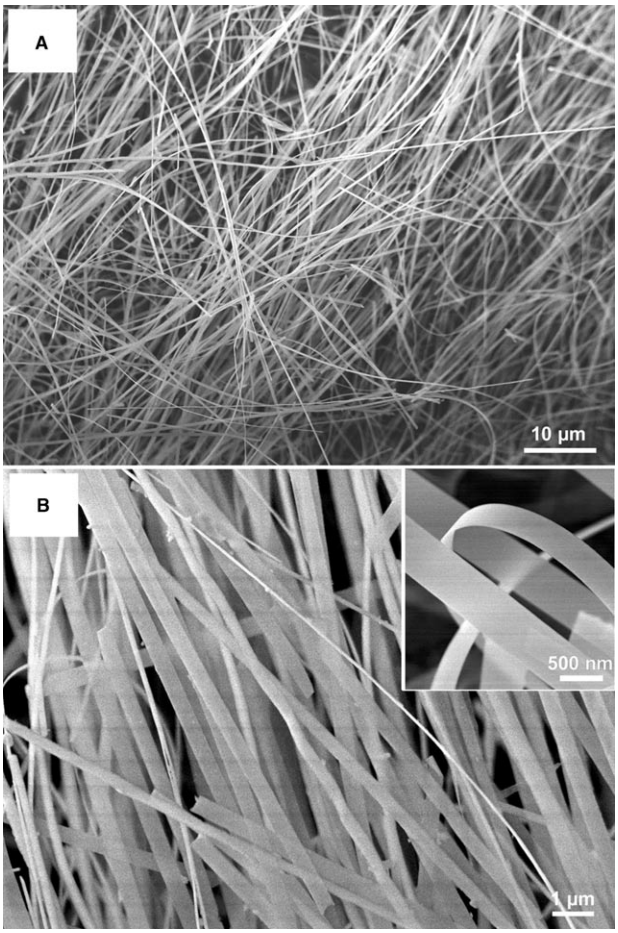

Figure 7. A) and B) SEM images with different magnifications of as-grown, wide α-Si_3N_4 nanoribbons. The upper right inset in B) shows the twisted ribbon shape.

electron energy loss (EEL) spectrum (Figure 6B), recorded by using a stationary focused 1 nm electron probe, shows the composition of the α-Si_3N_4 nanosaw. The peaks of the Si-$L_{2,3}$ edge (~99 eV) and N-K edge (~401 eV) indicate that the nanosaw is composed of Si and N. An insight into the structure of the nanosaw is revealed from high-resolution TEM (HRTEM) lattice images, which are displayed in Figures 6C and D. The *d* spacings of 0.56 and 0.67 nm in Figure 6D correspond well to the (001) and (010) plane, respectively, of α-Si_3N_4. Tens of nanosaws were checked and they gave the same results. Both the HRTEM images and the SAED patterns confirm the growth direction along the (011) plane. It is thought that the growth mechanism of the α-Si_3N_4 nanosaws produced in this work is similar to the structure reported in previous reports on wurtzite CdSe nanosaws; this mechanism was suggested to be a result of the polar surfaces.

Wide α-Si_3N_4 nanoribbons (S3): SEM images of the product deposited 8–9 cm away from the source material are shown in Figure 7. A low-magnification SEM image (Figure 7A) shows the formation of uniform, long, fiberlike nanostructures with lengths of up to several hundred of micrometers. Closer examination under high magnification (Figure 7B) reveals that the cross sections of the fiberlike nanostructures are rectangular; each fiber is 90 nm thick and 500 nm to several micrometers wide. Within each individual ribbon, the thickness and width are uniform along its entire length, when compared with those of α-Si_3N_4 nanosaws.

Figures 8A and B show the TEM images of several wide α-Si_3N_4 nanoribbons with typical diameters of about 2–3 μm. In accordance with the α-Si_3N_4 nanosaws obtained in this work, the wide α-Si_3N_4 nanoribbons are very thin and highly transparent to electrons; the copper grid can be seen through the wide nanoribbons. Ripplelike contrasts are clearly observed and are due to the strain resulting from bending of the structures. The SAED pattern (inset in Figure 8B) indicates the single-crystal nature of the wide α-Si_3N_4 nanoribbons. Typical HRTEM lattice images displayed in Figures 8C and D also indicate *d* spacings of 0.56 and 0.67 nm, corresponding well to the (001) and (010) planes, respectively, of α-Si_3N_4. This result is similar to that obtained with the α-Si_3N_4 nanosaws. The SAED and HRTEM

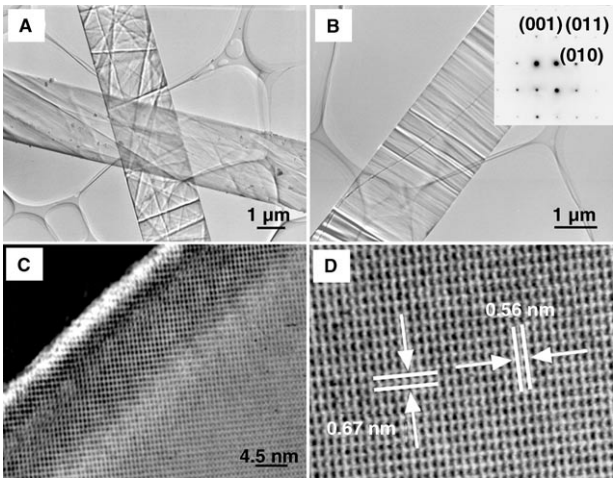

Figure 8. A) and B) Typical TEM images of wide and thin α-Si_3N_4 nanoribbons grown along the [011] direction with a width of several micrometers. C) and D) HRTEM lattice images of the wide nanobelts grown along the [011] direction. The *d* spacings of 0.56 and 0.67 nm in D) correspond well to the (001) and (010) planes of α-Si_3N_4.

results suggest that the wide α-Si_3N_4 nanoribbons grow along the [011] direction.

Narrow α-Si_3N_4 nanoribbons (S4): Investigation of the deposited product far from the source materials, about 9–11 nm, indicates that large-scale, narrow α-Si_3N_4 nanoribbons were obtained. Figure 9A is a low-magnification SEM image of the deposited product. The nanoribbons have quite narrow diameters, when compared with the above-analyzed, wide α-Si_3N_4 nanoribbons. The diameters of these nanoribbons range from 70 to 200 nm and their length is in the hundred micrometer scale. The high-magnification SEM images in Figures 9B and C clearly show twisted ribbonlike shapes. The TEM image in Figure 9D also shows a narrow thickness relative to the width.

α-Si_3N_4 nanowires (S5): On the top of the graphite crucible, another kind of α-Si_3N_4 nanostructure, namely, α-Si_3N_4 nanowires, was deposited; the SEM image is shown in Figure 10A. Compared with the α-Si_3N_4 micro- and nanoribbons, which show rectangular cross sections, the high-magnification SEM image shown in Figure 10B indicates that they have round cross sections with typical diameters of 70–100 nm and lengths of up to several hundreds of micrometers.

Growth mechanism: From the HRTEM examination, it was found that no dislocation or planar defects, such as stacking faults or twins, exist in the nanobelts. This is different from the previously reported oxide nanoribbons that grow in the form of twin and stacking fault mechanisms. VS and VLS mechanisms have been widely used to explain the formation of 1D structures.[20] In our work, no catalytic metal was used, so we thought that the formation of 1D α-Si_3N_4 nanostructures could be nucleated by the VS mechanism. The formation of 1D α-Si_3N_4 nanostructures may be generally described as outlined in Equations (1) and (2).

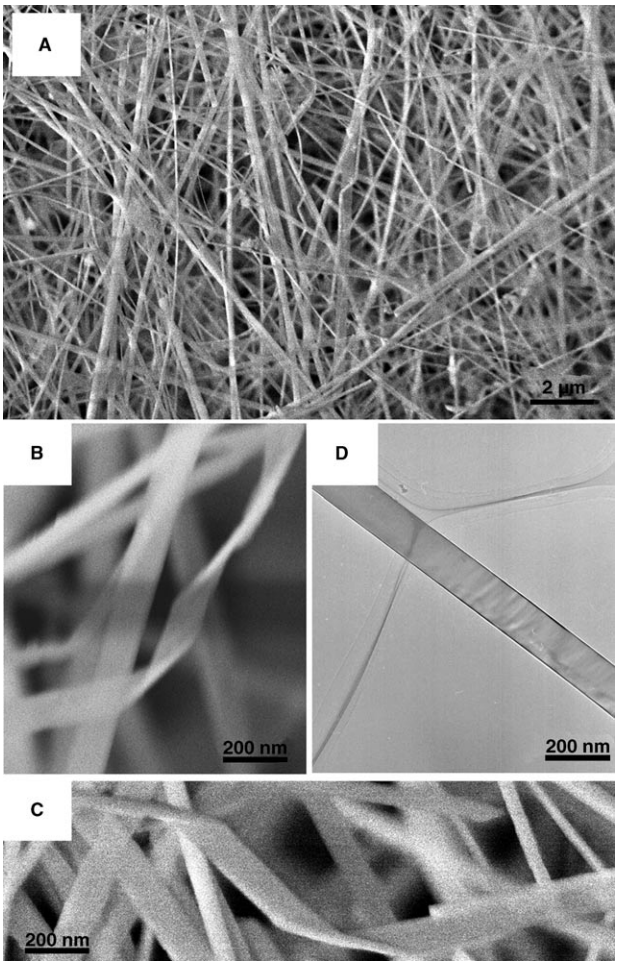

Figure 9. A) Low-magnification SEM image of as-grown, narrow α-Si_3N_4 nanoribbons. B) and C) High-magnification SEM images showing the twisted ribbon shapes. D) TEM image of the narrow α-Si_3N_4 nanoribbon.

$$2\,SiO \rightarrow Si + SiO_2 \quad (1)$$

$$3\,Si + 2\,N_2 \rightarrow Si_3N_4 \quad (2)$$

At high reaction temperatures, SiO tends to thermally decompose to Si and SiO_2. Si vapor is slowly produced in the reaction system. The newly generated Si vapor reacts with N_2 resulting in the formation of Si_3N_4 nanoclusters on the inner wall of the graphite crucible. These Si_3N_4 nanoclusters are energetically favorable and serve as stable sites for the adhesion of additional Si_3N_4 molecules. It is known that the surfaces with lower energy tend to grow larger and they remain flat even without atom steps at the growth temperature. Therefore, the low-energy surfaces determine the enclosure surfaces of the ribbons. In the deposition crucible, the gases vapor and concentration decrease as the distance between the source material and the deposition site increas-

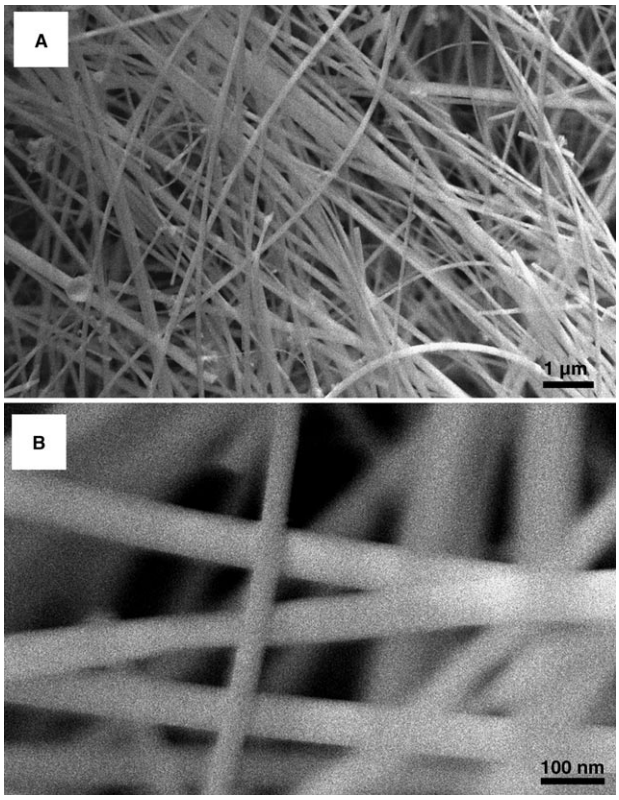

Figure 10. A) Low-magnification and B) high-magnification SEM images of the obtained α-Si_3N_4 nanowires.

es. At the deposition site near the source materials, in which the gases vapor and concentration are the highest, very wide and long microribbons are obtained. However, only narrow nanoribbons are formed far away from the source material due to a lack of vapor concentration. In the process, α-Si_3N_4 nanowires only deposit on the top of the crucible, for which the vapor concentration and the deposition temperature is the lowest. This result is in agreement with previous reports stating that higher temperature favors the formation of nanoribbons and lower temperature favors nanowires.[1b,12a,14b]

Photoluminescence (PL) properties: Since the observation of a strong visible PL in porous silicon at room temperature, light emission from Si-based devices has been an important research area for optoelectronic and display applications. This light-emission property plays an important role in the electronics industry, especially in Si-based large-scale integration circuit technology. Fundamentally speaking, an understanding of the electronic or optical properties of Si_3N_4 is of great interest. Previously, studies on Si_3N_4 show that there are four types of defects:[21] Si–Si and N–N bonds, and Si and N dangling bonds. The Si–Si bond forms a bonding σ orbital and antibonding σ* orbital that are separated by 4.6 eV in stoichiometric Si_3N_4. The silicon dangling bond forms a gap state about midgap#, and the two nitrogen defect states that give rise to levels within the gap, namely, N_4^+ and N_2^0, are near the conduction and valence bands, respectively. Figure 11 shows a comparison of the room-temperature PL spectra of α-Si_3N_4 nanosaws (Figure 11, spectrum A) and wide α-Si_3N_4 nanoribbons (Figure 11, spectrum B), respectively. Both samples show strong and broad emissions ranging from around 400 to 800 nm with two maximum peaks centered at 590 and 620 nm. This result is a little different from previous work on wide α-Si_3N_4 nanoribbons formed by VS thermal reaction between SiO and NH_3[16] (only one peak centered at 575 nm was observed), and from α-Si_3N_4 nanoribbons formed by catalytic-assisted pyrolysis of a polymeric precursor[15b] (three broad peaks centered at 1.8, 2.3, and 3.0 eV were observed). The exact mechanism needs to be studied further.

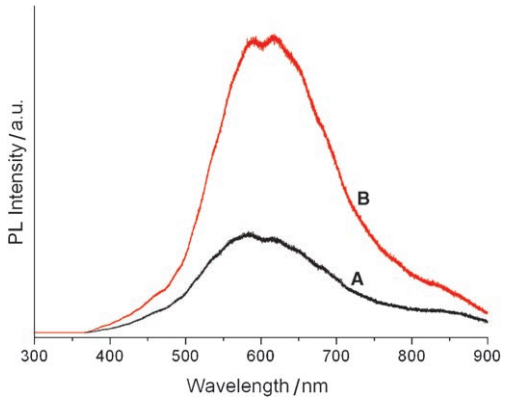

Figure 11. PL spectra of A) α-Si_3N_4 nanosaws and B) wide α-Si_3N_4 nanoribbons, showing a broad emission peak around 400–800 nm.

Conclusion

In this paper we have reported on the large-scale synthesis of 1D α-Si_3N_4 nanostructures by using a simple thermal-decomposition/nitridation method. Besides the formation of millimeter-scale α-Si_3N_4 microribbons, wide and narrow α-Si_3N_4 nanoribbons and nanowires, and α-Si_3N_4 nanosaws were also reported for the first time. Systematic investigation of these nanostructures by using XRD, SEM, TEM, and EELS indicates that all these nanostructures were of single crystalline nature and predominately grew along the [011] direction. These 1D nanostructures were formed by thermal decomposition, followed by the nitridation of SiO at high temperature in a nitrogen gas atmosphere; this procedure was dominated by a VS process. Room-temperature PL spectra of these nanostructures show broad visible emission at around 400–850 nm. The present study may provide not only more comprehensive insights into the formation mechanism of the nanostructures, but also a simple general approach to produce 1D nitride nanostructures with different morphologies.

Experimental Section

1D Si_3N_4 nanostructures were synthesized in a vertical induction furnace that consisted of a fused quartz tube and an induction-heated cylinder made of high-purity graphite coated with a C fiber thermoinsulating layer (Figure 1). The furnace had C inlet pipes on the top and base and C outlet pipes on the base. A specially designed graphite crucible, as shown in Figure 1, containing SiO (0.8 g) was placed in the center of the cylinder. After evacuation of the quartz tube to ~0.2 torr (1 torr = 133.322 pascal), a pure N_2 flow was passed through the carbon cylinder at a constant rate of 400 sccm from the top pipe and 600 sccm from the base pipe. The furnace was rapidly heated and kept at 1350 °C for 1 h. After the reaction was terminated and the furnace cooled to room temperature, the collected products were characterized by using XRD (RINT 2200) with $Cu_{K\alpha}$ radiation, SEM (JSM-6700F), and HRTEM (JEM-3000F). The PL measurements were conducted at room temperature by using a He–Cd laser line of 325 nm as the excitation source.

[1] a) Y. Huang, X. Duan, Q. Wei, C. M. Lieber, *Science* **2001**, *291*, 630–633; b) Z. Pan, Z. Dai, Z. L. Wang, *Science* **2001**, *291*, 1947–1949; c) M. Huang, S. Mao, H. Feick, H. Yan, Y. Wu, H. Kind, E. Weber, R. Russo, P. D. Yang, *Science* **2001**, *292*, 1897–1899.

[2] a) J. Q. Hu, Y. Bando, J. H. Zhan, D. Golberg, *Angew. Chem.* **2004**, *116*, 4706–4709; *Angew. Chem. Int. Ed.* **2004**, *43*, 4606–4609; b) C. C. Tang, Y. Bando, D. Golberg, R. Z. Ma, *Angew. Chem.* **2005**, *117*, 582–585; *Angew. Chem. Int. Ed.* **2005**, *44*, 576–579; c) J. Q. Hu, Y. Bando, D. Golberg, Q. L. Liu, *Angew. Chem.* **2003**, *115*, 3617–3621; *Angew. Chem. Int. Ed.* **2003**, *42*, 3493–3497.

[3] a) Y. N. Xia, P. D. Yang, Y. G. Sun, Y. Y. Wu, B. Mayer, B. Gates, Y. D. Yin, F. Kim, H. Q. Yan, *Adv. Mater.* **2003**, *15*, 353–389; b) Z. R. Dai, Z. W. Pan, Z. L. Wang, *Adv. Funct. Mater.* **2003**, *13*, 9–24; c) S. Iijima, *Nature* **1991**, *354*, 56–58.

[4] a) Y. Cui, C. M. Lieber, *Science* **2001**, *291*, 851–853; b) Y. C. Zhu, Y. Bando, L. W. Yin, *Adv. Mater.* **2004**, *16*, 331–334; c) D. D. Archibald, S. Mann, *Nature* **1993**, *364*, 430–433; d) S. Mann, G. A. Ozin, *Nature* **1996**, *382*, 313–318.

[5] a) R. E. Smalley, B. I. Yakobson, *Solid State Commun.* **1998**, *107*, 597–606; b) S. Iijima, T. Ichihashi, *Nature* **1993**, *363*, 603–605; c) X. G. Peng, L. Manna, W. D. Yang, J. Wickham, E. Scher, A. Kadavanich, A. P. Alivisatos, *Nature* **2000**, *404*, 59–61.

[6] a) C. P. Gibson, K. Putzer, *Science* **1995**, *267*, 1338–1340; b) T. S. Ahmadi, Z. L. Wang, T. C. Green, A. Henglein, M. A. El-sayed, *Science* **1996**, *272*, 1924–1926; c) M. P. Pileni, B. W. Ninham, T. Gulik-Krzywicki, J. Tanori, I. Lisiecki, A. Filankembo, *Adv. Mater.* **1999**, *11*, 1358–1362.

[7] S. Shimada, T. Kataoka, *J. Am. Ceram. Soc.* **2001**, *84*, 2442–2444.

[8] a) M. J. Hoffman, G. Petzow, *Mater. Res. Soc. Symp. Proc.* **1993**, *287*, 3–14; b) G. Ziegler, J. Heinrich, G. Wotting, *J. Mater. Sci.* **1987**, *22*, 3041–3086; c) R. K. Govila, *J. Mater. Sci.* **1985**, *20*, 4345–4353.

[9] a) Y. J. Zhang, N. L. Wang, R. R. He, Q. Zhang, J. Zhu, Y. J. Yan, *J. Mater. Res.* **2000**, *15*, 1048–1051; b) F. Munakata, K. Matsuo, K. Furuya, Y. J. Akimune, I. Ishikawa, *Appl. Phys. Lett.* **1999**, *74*, 3498–3500.

[10] a) W. Han, S. Fan, Q. Li, B. Gu, X. Zhang, D. Yu, *Appl. Phys. Lett.* **1997**, *71*, 2271–2273; b) L. D. Zhang, G. W. Meng, F. Phillipp, *Mater. Sci. Eng. A* **2000**, *286*, 34–38; c) G. Gundiah, G. V. Madhav, A. Govindaraj, M. M. Seikh, C. N. R. Rao, *J. Mater. Chem.* **2002**, *12*, 1606–1611; d) Y. H. Gao, Y. Bando, K. Kurashima, T. Sato, *Microsc. Microanal.* **2002**, *8*, 5–10.

[11] a) H. Kim, J. Park, H. Yang, *Chem. Phys. Lett.* **2003**, *372*, 269–274; b) C. Tang, X. Ding, X. Huan, Z. W. Gan, W. Liu, S. R. Qi, *Jpn. J. Appl. Phys. Part 2* **2002**, *41*, L589–L591; c) K. B. Tang, J. Q. Hu, Q. Lu, Y. Xie, J. Zhu, Y. T. Qian, *Adv. Mater.* **1999**, *11*, 653–655.

[12] a) G. Z. Shen, J. H. Cho, J. K. Yoo, G. C. Yi, C. J. Lee, *J. Phys. Chem. B* **2005**, *109*, 9294–9298; b) Z. P. Liu, J. B. Liang, S. Li, S. Peng, Y. T. Qian, *Chem. Eur. J.* **2004**, *10*, 634–640; c) Z. L. Wang, Z. W. Pan, *Adv. Mater.* **2002**, *14*, 1029–1032; d) M. S. Mo, J. H. Zeng, X. M. Liu, W. C. Yu, X. Y. Zhang, Y. T. Qian, *Adv. Mater.* **2002**, *14*, 1658–1662.

[13] a) S. Y. Bae, H. W. Seo, J. Park, H. Yang, J. C. Park, S. Y. Lee, *Appl. Phys. Lett.* **2002**, *81*, 126–128; b) Q. Wu, Z. Hu, X. Z. Wang, Y. Chen, Y. N. Lu, *J. Phys. Chem. B* **2003**, *107*, 9726–9729; c) L. Fu, Y. Q. Liu, P. Hu, K. Xiao, G. Yu, D. B. Zhu, *Chem. Mater.* **2003**, *15*, 4287–4291; d) X. B. Cao, Y. Xie, S. Y. Zhang, F. Q. Li, *Adv. Mater.* **2004**, *16*, 649–653.

[14] a) Y. Jiang, M. X. Meng, J. Liu, Z. Y. Xie, C. S. Lee, S. T. Lee, *Adv. Mater.* **2003**, *15*, 323–327; b) Q. Li, C. R. Wang, *Appl. Phys. Lett.* **2003**, *83*, 359–361; c) J. Q. Hu, X. L. Ma, N. G. Shang, Z. Y. Xie, N. B. Wong, C. S. Lee, S. T. Lee, *J. Phys. Chem. B* **2002**, *106*, 3823–3826.

[15] a) W. Y. Yang, Z. P. Xie, H. Z. Miao, L. G. Zhang, H. Ji, L. An, *J. Am. Ceram. Soc.* **2005**, *88*, 466–469; b) L. G. Zhang, J. Jin, W. Y. Yang, Z. P. Xie, H. Z. Miao, L. An, *Appl. Phys. Lett.* **2005**, *86*, 061908.

[16] L. W. Yin, Y. Bando, Y. C. Zhu, Y. B. Li, *Appl. Phys. Lett.* **2003**, *83*, 3584–3586.

[17] a) J. Q. Hu, Y. Bando, T. Sekiguchi, F. F. Xu, J. H. Zhan, *Appl. Phys. Lett.* **2004**, *84*, 804–806; b) J. Q. Hu, Y. Bando, Z. W. Liu, F. F. Xu, T. Sekiguchi, J. H. Zhan, *Chem. Eur. J.* **2004**, *10*, 554–558.

[18] a) C. Ma, D. Moore, Y. Ding, J. Li, Z. L. Wang, *Int. J. Nanotechnol.* **2004**, *1*, 431–451; b) C. Ma, Y. Ding, D. Moore, X. Wang, Z. L. Wang, *J. Am. Chem. Soc.* **2004**, *126*, 708–709; c) Z. L. Wang, X. Y. Kong, J. M. Zuo, *Phys. Rev. Lett.* **2003**, *91*, 185502; d) D. Moore, C. Roning, C. Ma, Z. L. Wang, *Chem. Phys. Lett.* **2004**, *385*, 8–11.

[19] S. Y. Bae, H. W. Seo, J. Park, H. Yang, *Chem. Phys. Lett.* **2003**, *373*, 620–625.

[20] a) R. S. Wagner, W. C. Ellis, *Appl. Phys. Lett.* **1964**, *4*, 89–91; b) X. F. Duan, C. M. Lieber, *J. Am. Chem. Soc.* **2000**, *122*, 188–189.

[21] a) J. Robertson, *Philos. Mag. B* **1991**, *63*, 44–47; b) P. A. Pundur, J. G. Shavalgin, V. A. Gritsenko, *Phys. Status Solidi A* **1986**, *94*, K107–K112; c) S. V. Deshpande, E. Gulari, S. W. Brown, S. C. Rand, *J. Appl. Phys.* **1995**, *77*, 6534–6541.

Received: August 2, 2005
Published online: January 23, 2006

